Inorg. Chem. **2005**, *44*, 6771–6776

Direct Determination of the Anisotropy and Exchange Splittings in the Dimeric Single-Molecule Magnet $[Mn_4O_3Cl_4(O_2CEt)_3(py)_3]_2 \cdot 8MeCN$ by Inelastic Neutron Scattering

Andreas Sieber,[†] Dolos Foguet-Albiol,[‡] Oliver Waldmann,[†] Stefan T. Ochsenbein,[†] Roland Bircher,[†] George Christou,[‡] Felix Fernandez-Alonso,[§] Hannu Mutka,[||] and Hans U. Güdel*,[†]

Departement für Chemie und Biochemie, Universität Bern, Freiestrasse 3, CH-3012 Bern, Switzerland, Department of Chemistry, University of Florida, Gainesville, Florida 32611, ISIS Facility, CCLRC Rutherford Appleton Laboratory, Chilton, Didcot, Oxfordshire OX11 0QX, UK, and Institut Laue-Langevin, 6 Rue Jules Horowitz, BP 156-38042, Grenoble Cedex 9, France

Received May 13, 2005

Energy splittings resulting from anisotropy and exchange interactions in the dimer of single-molecule magnets $[Mn_4O_3Cl_4(O_2CEt)_3(py)_3]_2 \cdot 8MeCN$ are determined for both an undeuterated and a partially deuterated sample using inelastic neutron scattering. The antiferromagnetic (AF) exchange coupling between the two Mn_4 subunits strongly depends on their separation. The Cl···Cl distance between the two subunits can be modified either by exchanging the solvent of crystallization or by deuteration of the C–H···Cl hydrogen bonds. The exchange of acetonitrile for *n*-hexane leads to a five times greater shortening of the Cl···Cl separation than does full deuteration of all the hydrogen bonds. As a result, the AF exchange coupling constants between the subunits are 0.0073(4) and 0.0103(9) meV in the samples with acetonitrile and *n*-hexane solvent molecules, respectively, in the crystal structure. On the other hand, the effect of C–H···Cl deuteration on the AF exchange coupling is not detectable within the experimental accuracy of INS.

Introduction

Single-molecule magnets (SMMs) are a class of inorganic compounds that continue to attract a great deal of scientific attention.[1] They are exchange-coupled polynuclear complexes of transition metal ions exhibiting phenomena such as slow relaxation and quantum tunneling of the magnetization (QTM) at very low temperatures.[2,3] Potentially, a single bit of information can be stored magnetically on such molecules at liquid helium temperatures, and this has naturally raised hopes of technological applications.[4] Although the SMM phenomena were first discovered about 15 years ago,[5−7] this research has thus far not led to any technological breakthroughs. The phenomenon is reasonably well understood by now, and dozens of new spin clusters exhibiting SMM behavior at liquid helium temperatures have been reported.[3,5,8−11] One of the main problems is that the so-called

* To whom correspondence should be addressed. E-mail: hans-ulrich.guedel@iac.unibe.ch.
[†] Universität Bern.
[‡] University of Florida.
[§] ISIS Facility.
[||] Institut Laue-Langevin.

(1) Christou, G.; Gatteschi, D.; Hendrickson, D. N.; Sessoli, R. *MRS Bull.* **2000**, *25*, 66−71.
(2) (a) Gatteschi, D.; Sessoli, R. *Angew. Chem., Int. Ed.* **2003**, *42*, 268−297. (b) Basler, R.; Boskovic, C.; Chaboussant, G.; Güdel, H. U.; Murrie, M.; Ochsenbein, S. T.; Sieber, A. *Chem. Phys. Chem.* **2003**, *4*, 910−926. (c) Chudnovsky, E. M.; Tejada, J. *Macroscopic Quantum Tunneling of the Magnetic Moment*; Cambridge University Press: Cambridge, UK, 1998.
(3) Sessoli, R.; Gatteschi, D.; Caneschi, A.; Novak, M. A. *Nature* **1993**, *365*, 141−143.
(4) (a) Cornia, A.; Fabretti, A. C.; Pacchioni, M.; Zobbi, L.; Bonacchi, D.; Caneschi, A.; Gatteschi, D.; Biagi, R.; Del Pennino, U.; De Renzi, V.; Gurevich, L.; Van der Zant, H. S. J. *Angew. Chem., Int. Ed.* **2003**, *42*, 1645−1648. (b) Aubin, S. M. J.; Eppley, H. J.; Christou, G.; Hendrickson, D. N. *Book of Abstracts*, 213th ACS National Meeting, San Francisco, April 13−17 1997; American Chemical Society: Washington, D.C., 1997; INOR-419. (c) Leuenberger, M. N.; Loss, D. *Nature* **2001**, *410*, 789−793.
(5) Caneschi, A.; Gatteschi, D.; Sessoli, R.; Barra, A. L.; Brunel, L. C.; Guillot, M. *J. Am. Chem. Soc.* **1991**, *113*, 5873−5874.
(6) Thomas, L.; Lionti, F.; Ballou, R.; Gatteschi, D.; Sessoli, R.; Barbara, B. *Nature* **1996**, *383*, 145−147.
(7) Friedman, J. R.; Sarachik, M. P.; Tejada, J.; Ziolo, R. *Phys. Rev. Lett.* **1996**, *76*, 3830−3833.
(8) Aubin, S. M. J.; Dilley, N. R.; Pardi, L.; Krzystek, J.; Wemple, M. W.; Brunel, L. C.; Maple, M. B.; Christou, G.; Hendrickson, D. N. *J. Am. Chem. Soc.* **1998**, *120*, 4991−5004.

10.1021/ic050764l CCC: $30.25
Published on Web 08/16/2005

blocking temperature (T_B), below which information could be stored magnetically, is still extremely low. Mn_{12}-acetate, the first reported SMM, still has the highest T_B, of the order of about 3 K.[6]

It is no wonder that many scientists are exploring new avenues to create systems exhibiting SMM phenomena.[12,13] One of these has led to the discovery of a new type of hysteresis in the title compound.[12] $[Mn_4O_3Cl_4(O_2CEt)_3(py)_3]_2 \cdot 8MeCN$, or $(Mn_4)_2$ in short, consists of two identical Mn_4 clusters joined by weak C−H···Cl hydrogen bonds[11] (Figure 1). A whole family of Mn_4 clusters with the formula $[Mn_4O_3(OAc)_3X(dbm)_3]$ (X varies; F, Cl, Br, OAc, or $OSi(CH_3)_3$) have been reported and characterized as SMMs below 2 K.[8,9,14] The $(Mn_4)_2$ dimer still shows slow relaxation and QTM at these low temperatures, but efficient QTM does not occur at the same magnetic fields as for the uncoupled Mn_4 molecules. In particular, there is no tunneling at zero magnetic field,[12] in contrast to all other SMMs. This deviation can be readily explained by weak antiferromagnetic (AF) exchange interactions between the two Mn_4 subunits, mediated by the C−H···Cl hydrogen bonds and the close Cl···Cl approach of 3.878 Å.[12,15]

The strength of this AF exchange coupling has been quantified from low-temperature magnetic[12] and EPR measurements.[15] The present study had two objectives: to accurately determine the exchange splittings and thus the exchange parameter and to quantify the effect of deuteration of the hydrogen bonds on the coupling strength. The method used was high-resolution inelastic neutron scattering (INS),

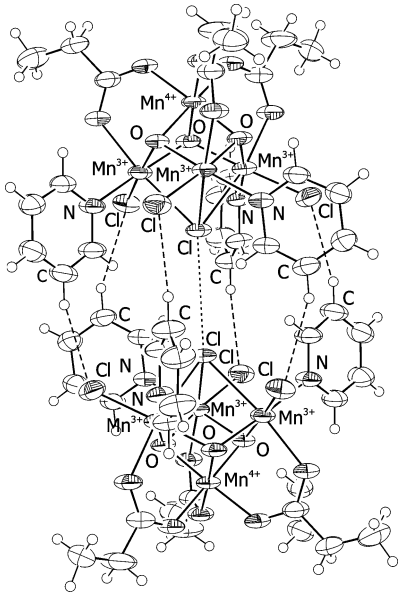

Figure 1. Structure of $[Mn_4O_3Cl_4(O_2CEt)_3(py)_3]_2$. The two Mn_4 subunits are held together by six C−H···Cl hydrogen bonds (dotted lines). The weak antiferromagnetic exchange coupling between the two subunits is mediated by these hydrogen bonds and the close Cl···Cl approach (dashed lines).

which had been successfully employed to accurately determine the anisotropy parameters in the ground state of several Mn_4 SMM clusters.[14]

Experimental Section

INS experiments were performed on IRIS at the ISIS Facility, CCLRC Rutherford Appleton Laboratory in Chilton, UK, and on IN5 at the Institut Laue-Langevin (ILL) in Grenoble, France. Spectra were acquired in the temperature range of 1.5−20 K on 4.4 g of an undeuterated ($[Mn_4O_3Cl_4(O_2CEt)_3(py)_3]_2 \cdot 8MeCN$) and a partially deuterated ($[Mn_4O_3Cl_4(O_2CEt)_3(py\text{-}d_5)_3]_2 \cdot 8MeCN$) microcrystalline sample of $(Mn_4)_2$ sealed in an annular-shaped aluminum cylinder with dimensions of $d_{in} = 20$ mm, $d_{out} = 24$ mm, and $h = 50$ mm (IRIS) and $d_{in} = 9$ mm, $d_{out} = 15$ mm, and $h = 50$ mm (IN5). On IRIS, the spectra of both, the partially deuterated and undeuterated compounds, were recorded using a pyrolytic graphite (PG002) analyzer with a final wavelength of $\lambda_f = 6.6$ Å (FWHM = 17.5 μeV at zero energy transfer) in the energy-transfer range from −0.3 to 1.2 meV. The accessible Q range was 0.4 to 1.6 $Å^{-1}$. The time-of-flight to energy conversion and reduction of IRIS data were done with the ISIS Facility analysis packages IDA and MSLICE.[16] The IN5 data were measured on an undeuterated sample with an incident wavelength of $\lambda_i = 7.0$ Å corresponding to a FWHM = 31 μeV at zero energy transfer. The energy transfer range was −0.9 to 1.1 meV with an accessible Q range from 0.2 to 1.6 $Å^{-1}$. The time-of-flight to energy conversion and the data reduction employed the standard program INX (ILL). The data were corrected for detector efficiency by means of a spectrum of vanadium metal. In both experiments, the data correspond to the sum of all available detectors. Further data treatment included subtraction of the background by approximating it with a suitable analytical function.

For both experiments, the samples were freshly prepared according to ref 11 and were checked by X-ray powder diffraction,

(9) Aubin, S. M. J.; Wemple, M. W.; Adams, D. M.; Tsai, H. L.; Christou, G.; Hendrickson, D. N. *J. Am. Chem. Soc.* **1996**, *118*, 7746−7754.
(10) (a) Sessoli, R.; Tsai, H. L.; Schake, A. R.; Wang, S. Y.; Vincent, J. B.; Folting, K.; Gatteschi, D.; Christou, G.; Hendrickson, D. N. *J. Am. Chem. Soc.* **1993**, *115*, 1804−1816. (b) Eppley, H. J.; Tsai, H. L.; Devries, N.; Folting, K.; Christou, G.; Hendrickson, D. N. *J. Am. Chem. Soc.* **1995**, *117*, 301−317. (c) Villain, J.; Hartmanboutron, F.; Sessoli, R.; Rettori, A. *Europhys. Lett.* **1994**, *27*, 159−164. (d) Wemple, M. W.; Adams, D. M.; Folting, K.; Hendrickson, D. N.; Christou, G. *J. Am. Chem. Soc.* **1995**, *117*, 7275−7276. (e) Wemple, M. W.; Adams, D. M.; Hagen, K. S.; Folting, K.; Hendrickson, D. N.; Christou, G. *J. Chem. Soc., Chem. Commun.* **1995**, 1591−1593. (f) Wang, S. Y.; Folting, K.; Streib, W. E.; Schmitt, E. A.; McCusker, J. K.; Hendrickson, D. N.; Christou, G. *Angew. Chem., Int. Ed.* **1991**, *30*, 305−306. (g) Wang, S. Y.; Tsai, H. L.; Libby, E.; Folting, K.; Streib, W. E.; Hendrickson, D. N.; Christou, G. *Inorg. Chem.* **1996**, *35*, 7578−7589. (h) Wemple, M. W.; Tsai, H. L.; Folting, K.; Hendrickson, D. N.; Christou, G. *Inorg. Chem.* **1993**, *32*, 2025−2031.
(11) Hendrickson, D. N.; Christou, G.; Schmitt, E. A.; Libby, E.; Bashkin, J. S.; Wang, S. Y.; Tsai, H. L.; Vincent, J. B.; Boyd, P. D. W.; Huffman, J. C.; Folting, K.; Li, Q. Y.; Streib, W. E. *J. Am. Chem. Soc.* **1992**, *114*, 2455−2471.
(12) Wernsdorfer, W.; Allaga-Alcalde, N.; Hendrickson, D. N.; Christou, G. *Nature* **2002**, *416*, 406−409.
(13) (a) Ishikawa, N.; Sugita, M.; Wernsdorfer, W. *J. Am. Chem. Soc.* **2005**, *127*, 3650−3651. (b) Mishra, A.; Wernsdorfer, W.; Parsons, S.; Christou, G.; Brechin, E. *Chem. Commun.* **2005**, 54−56; (c) Ferbinteanu, M.; Miyasaka, H.; Wernsdorfer, W.; Nakata, K.; Sugiura, K.-I.; Yamashita, M.; Coulon, C.; Clerac, R. *J. Am. Chem. Soc.* **2005**, *127*, 3090−3099. (d) Chakov, N. E.; Wernsdorfer, W.; Abboud, K. A.; Christou, G. *Inorg. Chem.* **2004**, *43*, 5919−5930. (e) Miyasaka, H.; Clerac, R.; Mizushima, K.; Sugiura, K.-i.; Yamashita, M.; Wernsdorfer, W.; Coulon, C. *Inorg. Chem.* **2003**, *42*, 8203−8213. (f) Clerac, R.; Miyasaka, H.; Yamashita, M.; Coulon, C. *J. Am. Chem. Soc.* **2002**, *124*, 12837−12844.
(14) Andres, H.; Basler, R.; Güdel, H. U.; Aromi, G.; Christou, G.; Buttner, H.; Ruffle, B. *J. Am. Chem. Soc.* **2000**, *122*, 12469−12477.
(15) Hill, S.; Edwards, R. S.; Aliaga-Alcalde, N.; Christou, G. *Science* **2003**, *302*, 1015−1018.
(16) Adams, M. A.; Howells, W. S.; Telling, M. T. F. *The IRIS User Guide*, 2nd ed.; Technical Report RAL-TR-2001-002; Rutherford Appleton Laboratory: Oxfordshire, U.K., 2001.

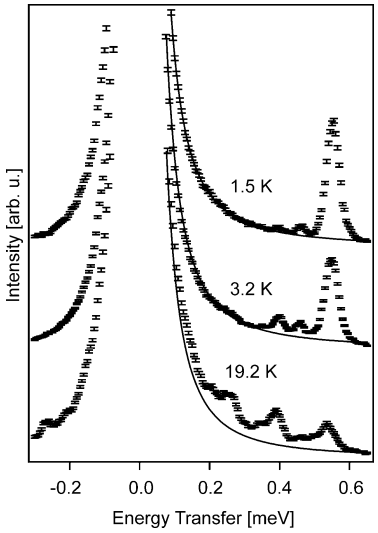

Figure 2. INS spectra at 1.5, 3.2, and 19.2 K of a partially deuterated polycrystalline sample of $(Mn_4)_2$ recorded on IRIS with a final wavelength $\lambda_f = 6.6$ Å. The spectra correspond to the sum of all scattering angles. The solid line represents the background.

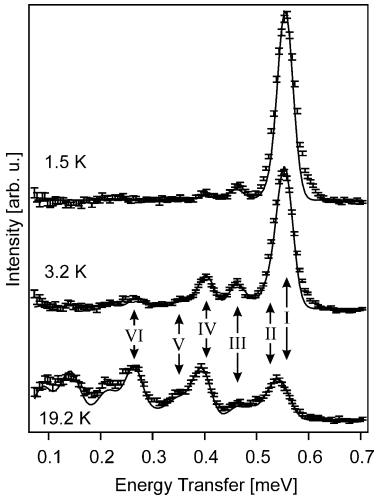

Figure 3. INS spectra at 1.5, 3.2, and 19.2 K of a partially deuterated polycrystalline sample of $(Mn_4)_2$ recorded on IRIS with a final wavelength $\lambda_f = 6.6$ Å after background subtraction. The labeling of the peaks corresponds to that in Figure 5. The solid lines represent the simulated spectra with the following parameters: $D = -0.0626(5)$ meV, $B_4^0 = -6.8(4) \times 10^{-6}$ meV, $J = 0.0072(4)$ meV, and FWHM = 0.035 meV.

elemental analysis, and variable-temperature dc magnetization measurements.

Results

Figure 2 shows the INS spectra of the partially deuterated sample at 1.5, 3.2, and 19.2 K, measured on the inverted geometry time-of-flight spectrometer IRIS at the ISIS facility. The solid lines in Figure 2 represent a smooth background that accounts for the finite instrumental resolution as well as elastic and quasielastic scattering from the sample not associated with magnetic INS transitions. The neutron energy loss side of the spectra after background subtraction is shown in Figure 3. At 1.5 K, one strong peak (I) at 0.56 meV and two weaker features (III, IV) at lower energies are observed. The intensity of peak I is almost constant as a function of Q. The Q dependence is most likely smeared out because of

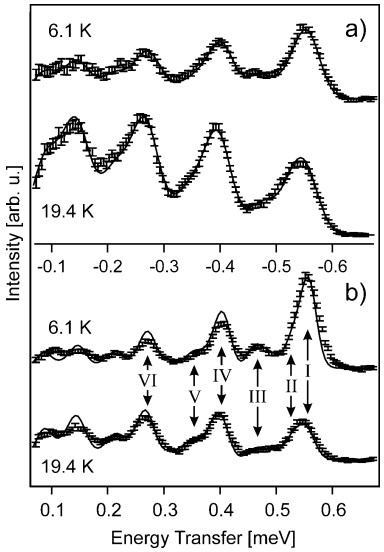

Figure 4. INS spectra at 6.1 and 19.4 K of an undeuterated polycrystalline sample of $(Mn_4)_2$ recorded on IN5 with an initial wavelength $\lambda_i = 7.0$ Å after background subtraction: (a) energy gain side and (b) energy loss side. The labeling of the peaks corresponds to that in Figure 5. The solid lines represent the simulated spectra with the following parameters: $D = -0.0629(5)$ meV, $B_4^0 = -6.8(4) \times 10^{-6}$ meV, $J = 0.0073(4)$ meV, FWHM = 0.031 meV (loss side), and FWHM = 0.05 meV (gain side).

the high hydrogen content of the sample. At elevated temperatures, the intensity of the cold peak (I) decreases, and several partially resolved hot peaks at lower energies are observed. Peak I broadens with increasing temperature, and the maximum shifts slightly to lower energy. This indicates that peak I is composed of several transitions at elevated temperatures.

Figure 4 shows the INS spectra of the undeuterated sample at 6.1 and 19.4 K after background subtraction. These spectra were measured on the direct geometry time-of-flight spectrometer IN5 at the ILL, both on the energy gain (Figure 4a) and energy loss (Figure 4b) side. The undeuterated compound was also measured on IRIS at 1.5, 3.2, and 19.2 K (not shown). The data are very similar to those of the partially deuterated compound (Figure 3).

Analysis

The Mn_4 subunits consist of one Mn^{4+} ($S = 3/2$) and three Mn^{3+} ($S = 2$) ions, which form a distorted cubane structure as depicted in Figure 1. The dominant AF exchange coupling between the Mn^{4+} ion and each of the Mn^{3+} ions in the subunit leads to a well-isolated total spin $S = 9/2$ ground state for each Mn_4 subunit. Jahn−Teller distortions of the Mn^{3+} ions introduce an easy axis-type magnetic anisotropy along the trigonal axis of the cluster.[11] The $S = 9/2$ ground state is thus split into five $\pm M_S$ Kramers doublets. This splitting can be described by the effective zero-field splitting Hamiltonian

$$\hat{H}_{ZFS} = D\left[\hat{S}_z^2 - \frac{1}{3}S(S+1)\right] + B_4^0\hat{O}_4^0 \qquad (1)$$

where $\hat{O}_4^0 = 35\hat{S}_z^4 - 30S(S+1)\hat{S}_z^2 + 25\hat{S}_z^2 + 6S(S+1)$.

The leading term is the D term, with a negative D value of the order of $D \approx -0.06$ meV for all the known Mn_4

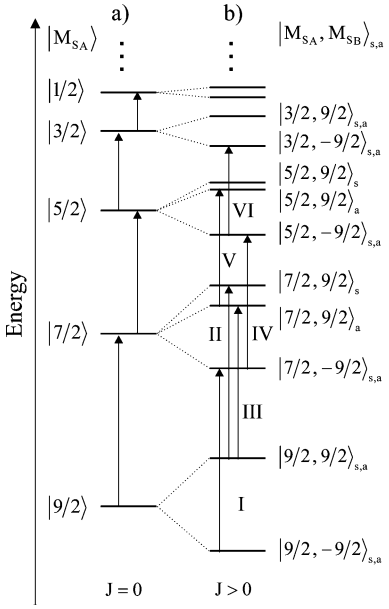

Figure 5. Energy level diagram of (a) an axially anisotropy split $S = 9/2$ ground state (eq 1 with $D = -0.063$ meV and $B_4^0 = -6.8 \times 10^{-6}$ meV) of a Mn_4 subunit and (b) a $(Mn_4)_2$ dimer with antiferromagnetic coupling (eq 2 with $D = -0.063$ meV, $B_4^\circ = -6.8 \times 10^{-6}$ meV, and $J = 0.0073$ meV). For clarity only the relevant states are shown. The arrows in panel b correspond to the assignments of the observed transitions in Figures 3 and 4. The approximate wave functions are given for $M_{SA} > 0$ in the following notation $|M_{SA},M_{SB}\rangle_s = (|M_{SA},M_{SB}\rangle + |M_{SB},M_{SA}\rangle)/\sqrt{2}$, $|M_{SA},M_{SB}\rangle_a = (|M_{SA},M_{SB}\rangle - |M_{SB},M_{SA}\rangle)/\sqrt{2}$.

SMMs.[8,14] The resulting splitting pattern is shown in Figure 5a. In the title compound, two identical Mn_4 molecules are lying head-to-head on a crystallographic S_6 axis. In terms of anisotropy, the two subunits are thus equivalent and represented by the same parameters as in eq 1. A small perturbation is introduced by the exchange coupling between the two subunits, leading to the following effective Hamiltonian for the dimer

$$\hat{H} = \hat{H}_{ZFS,A} + \hat{H}_{ZFS,B} + J\hat{S}_A\hat{S}_B \qquad (2)$$

where $\hat{H}_{ZFS,\nu}$ are centered on the two subunits A and B, respectively, and have the form of eq 1. The effect of a positive (antiferromagnetic) J value on the ground-state splitting is seen in Figure 5b. All the Kramers doublets of the Mn_4 subunits are split into two or three components. In the first order, the dimer wave functions are given by the symmetric $|M_{SA},M_{SB}\rangle_s = (|M_{SA},M_{SB}\rangle + |M_{SB},M_{SA}\rangle)/\sqrt{2}$ and antisymmetric $|M_{SA},M_{SB}\rangle_a = (|M_{SA},M_{SB}\rangle - |M_{SB},M_{SA}\rangle)/\sqrt{2}$ linear combinations of the basis functions, with $M_S = M_{SA} + M_{SB}$. INS transitions are allowed for $\Delta M_S = \pm 1,0$. In the first order description, this corresponds specifically to $\Delta M_{SA} = \pm 1$ and $\Delta M_{SB} = 0$ or $\Delta M_{SA} = 0$ and $\Delta M_{SB} = \pm 1$. The experimentally assigned allowed transitions within the energy level diagram of Figure 5b are shown as arrows and labeled I through VI. On the basis of their temperature dependence, the major peaks in the INS spectra of Figures 3 and 4 can be assigned to the allowed transitions I−VI in Figure 5b. From the resulting energy-splitting pattern, the relevant parameters in eq 2 can be determined approximately.

Since some of the observed peaks consist of more than one transition, we included the relative intensities of the INS transitions, in addition to their energies, for a more accurate determination. The INS cross section for a transition $|n\rangle \rightarrow |m\rangle$ ($|n\rangle$ and $|m\rangle$ denote eigenstates of the Hamiltonian eq 2) is proportional to the thermal population of the initial level $|n\rangle$ and the transition strength $I_{nm}(\mathbf{Q})$ (or $I_{nm}(Q)$ for a polycrystalline sample), where $\mathbf{Q} = \mathbf{k} - \mathbf{k}'$ is the momentum transfer with $\mathbf{k}$ and $\mathbf{k}'$ defined as the initial and final wavevectors, respectively. In the calculation of $I_{nm}(Q)$, the geometry of the cluster enters via the so-called interference factors.[17] Since the $(Mn_4)_2$ cluster is described magnetically by an effective dimer model, see eq 2, a simple application of the INS cross section formula would miss important interference effects, and yield incorrect INS intensities. The interference effects, however, can be retained in the dimer model as described in ref 18, and for a polycrystalline sample of the uniaxial $(Mn_4)_2$ dimer $I_{nm}(Q)$ is obtained as

$$I_{nm}(Q) = \frac{2}{3}\sum_{\nu\mu\in\{A,B\}}[f_{\nu\mu}(Q,\mathbf{R}_{ij})(\tilde{S}_{\nu x}\tilde{S}_{\mu x} + \tilde{S}_{\nu y}\tilde{S}_{\mu y}) + g_{\nu\mu}(Q,\mathbf{R}_{ij})\tilde{S}_{\nu z}\tilde{S}_{\mu z}] \quad (3)$$

with

$$f_{\nu\mu}(Q,\mathbf{R}_{ij}) = \frac{1}{16}\sum_{i\in\nu}\sum_{j\in\mu}F_i^*F_j\left[j_0(QR_{ij}) - \frac{1}{2}C_0^{\,2}(\mathbf{R}_{ij})j_2(QR_{ij})\right]$$

and

$$g_{\nu\mu}(Q,\mathbf{R}_{ij}) = \frac{1}{16}\sum_{i\in\nu}\sum_{j\in\mu}F_i^*F_j[j_0(QR_{ij}) + C_0^{\,2}(\mathbf{R}_{ij})j_2(QR_{ij})]$$

and

$$\tilde{S}_{\nu\alpha}\tilde{S}_{u\beta} \equiv \langle n|\hat{S}_{\nu\alpha}|m\rangle\langle m|\hat{S}_{u\beta}|n\rangle$$

where ν and μ index the subunits A and B and i and j represent the individual Mn ions in the cluster. $F_i(Q)$ is the magnetic form factor of the ith ion, j_k is the spherical Bessel function of order k, $\mathbf{R}_{ij} = \mathbf{R}_i - \mathbf{R}_j$ is the distance vector between the ith and jth ion, $C_0^{\,2}(\mathbf{R}_{ij}) \equiv [3(R_{ij,z}/R_{ij})^2 - 1]/2$ and $\alpha, \beta = x, y, z$.

On the basis of eq 3, a least-squares fit of the calculated INS spectra, assuming Gaussian line shapes, to the experimental data at all the measured temperatures was performed. The results are shown as solid lines in Figures 3 and 4 for the deuterated and undeuterated samples, respectively. The agreement of the simulated and observed spectra is excellent for both samples at all temperatures. The parameters obtained are shown in Table 1. Within experimental accuracy, there is no significant difference between the two parameter sets.

An interesting question is whether the exchange interaction between the two subunits is isotropic or not.[15] To first order, the effect of the J_{xy} components of the exchange coupling is to split the two levels $|7/2,9/2\rangle_s$ and $|7/2,9/2\rangle_a$ by $9J_{xy}$. All

(17) (a) Furrer, A.; Güdel, H. U. *Phys. Rev. Lett.* **1977**, *39*, 657−660. (b) Waldmann, O. *Phys. Rev. B* **2003**, *68*, 174406/1−8.
(18) Waldmann, O.; Dobe, C.; Mutka, H.; Güdel, H. U. To be published.

Table 1. Spin Hamiltonian Parameters for the Deuterated and Undeuterated $(Mn_4)_2$ Dimer

	meV		
	D	B_4^0	J
deuterated	−0.0626(5)	$-6.8(4) \times 10^{-6}$	0.0072(4)
undeuterated	−0.0629(5)	$-6.8(4) \times 10^{-6}$	0.0073(4)

the other energy splittings of the Kramers doublets result from the J_z component of the exchange interaction. Since the J_{xy} component affects such a small portion of the spectrum, the introduction of exchange anisotropy does not significantly improve a least-squares fit to the whole spectrum. However, from the energy difference between transition II and III, which is related to the splitting of the $|7/2,9/2\rangle_{s,a}$ levels, J_{xy} can be directly determined. Transition III is nicely resolved at 3.2 K, whereas transition II lies in the lower-energy tail of peak I. This can be seen in the broadening and slight shift of the maximum of peak I to lower energy with increasing temperature. Peak III has an energy of 0.463(5) meV, and the energy of transition II is estimated to 0.530(15) meV. Their energy difference of 0.065(20) meV corresponds to $J_{xy} = 0.007(2)$ meV. Within experimental accuracy, there is no difference to the isotropic J value of 0.0072(4) meV, indicating isotropic exchange.

Discussion

According to the X-ray diffraction data, the geometries of the Mn_4 subunits in the deuterated and undeuterated title compounds are not distinguishable. But the Cl···Cl separation of the two subunits is slightly different: Cl···Cl distances of 3.844(3) and 3.878(4) Å at 173 K have been reported for the deuterated and undeuterated crystals, respectively.[19] We thus intuitively expect a stronger exchange coupling in the deuterated sample. The INS data analysis allows J to be determined within an accuracy of ±5%. Since no significant difference for the two samples is found, we conclude that the increase of J upon deuteration is at most 5%.

The samples used in the present study contained 8 molecules of acetonitrile per $(Mn_4)_2$ dimer in the crystal structure. This was the solvent used for the crystallization. This sample was studied in great detail by very low-temperature magnetic measurements,[12] and a value of $J =$ 0.0086 meV was derived from these, which is somewhat larger than the J value obtained by INS. The spectroscopic value is considered more reliable because it results from a direct observation of energy splittings.

An EPR study of the same $(Mn_4)_2$ dimer was performed on a sample containing 2 molecules of *n*-hexane, instead of acetonitrile, as the solvent of crystallization.[15] A value for J_{hexane} of 0.0103(9) meV was determined for this sample. This is significantly larger than the value for $J_{acetonitrile}$ of 0.073(4) meV obtained in the present study. An inspection of the crystal structures shows a significant shortening of the Cl···Cl separation in the EPR sample: $d_{Cl\cdots Cl} = 3.712$-(2) Å versus $d_{Cl\cdots Cl} = 3.86$ Å for the average of the INS samples.[19] The difference between the two samples containing different solvent molecules is significantly larger than the difference between the deuterated and undeuterated versions of the title compound. And we observe the intuitively expected trend: stronger antiferromagnetic exchange for the sample with the shorter Cl···Cl distance. The relevant numbers are collected in Table 2.

Table 2. Cl···Cl Distances and J Values for the Three Different $(Mn_4)_2$ Samples

	Å	meV		
sample[a]	Cl···Cl	J_{magn}[b]	J_{INS}	J_{EPR}[c]
1	3.878(4)	0.0086	0.0073(4)	
2	3.844(3)		0.0072(4)	
3	3.712(2)			0.0103(9)

[a] 1, $[Mn_4O_3Cl_4(O_2CEt)_3(py)_3]_2 \cdot 8MeCN$ (undeuterated); 2, $[Mn_4O_3Cl_4(O_2CEt)_3(py\text{-}d_5)_3]_2 \cdot 8MeCN$ (deuterated); 3, $[Mn_4O_3Cl_4(O_2CEt)_3(py)_3]_2 \cdot 2C_6H_{14}$. [b] From ref 12. [c] From ref 15.

This is a very interesting result because it demonstrates that the distance between the two subunits in the $(Mn_4)_2$ dimer, and thus, the strength of the exchange coupling between the subunits is more strongly affected by exchanging the solvent molecules situated between the $(Mn_4)_2$ dimers in the crystal structure than by deuterating the C−H···Cl hydrogen bonds connecting the Mn_4 subunits within the dimers. The effect of the solvent exchange on the Cl···Cl distance is about five times as large as the effect of deuteration. And the antiferromagnetic J value is about 40% larger in the sample with *n*-hexane solvent molecules. In the theory of kinetic exchange, the antiferromagnetic J value is related to a one-electron transfer integral, which, in turn, is related to the orbital overlap integrals. For two approaching subunits, as in the title compound, the distance dependence of J at long distances is given by e^{-kd}, where d is the distance between the subunits. [20,21]

Taking the Cl···Cl distance as d and the spectroscopically determined J values in Table 2, a value of $k = 2.5(9)$ is obtained. This is in reasonable agreement with the result of a recent DFT calculation on the title compound which derived $k = 4.5$.[21]

The fact that solvent exchange has a stronger effect on both the structure and the exchange coupling than deuteration is a reflection of the intrinsic weakness of the C−H···Cl hydrogen bonds. Despite this weakness, the six C−H···Cl bonds manage to structurally join together the two Mn_4 subunits in the title compound,[22] and they may well play an important role as pathways for the small superexchange between the Mn_4 subunits.

Conclusions

The anisotropy and exchange splitting in the exchange-coupled dimer of SMMs $(Mn_4)_2$ could be accurately determined by INS. The weak antiferromagnetic exchange interaction between the two Mn_4 subunits within the dimer

(19) Unpublished results.

(20) Anderson, P. W. *Solid State Phys.* **1963**, *14*, 99−214.
(21) Park, K.; Pederson, M. R.; Richardson, S. L.; Aliaga-Alcalde, N.; Christou, G. *Phys. Rev. B* **2003**, *68*, 020405/1−4.
(22) (a) Desiraju, G. R. *Acc. Chem. Res.* **1996**, *29*, 441−449. (b) Freytag, M.; Jones, P. G. *Chem. Commun.* **2000**, 277−278. (c) Aullon, G.; Bellamy, D.; Brammer, L.; Bruton, E. A.; Orpen, A. G. *Chem. Commun.* **1998**, 653−654.

strongly depends on the intradimer distance. This distance can be chemically modified either by exchanging the solvent of crystallization or by deuteration of the six hydrogen bonds connecting the two subunits. Deuteration of the weak hydrogen bonds has no measurable influence on the exchange coupling (below 5%), although it slightly shortens the intradimer separation. The substitution of acetonitrile by *n*-hexane considerably shortens the intradimer distance, increasing the exchange coupling by about 40%.

Acknowledgment. This work was funded by the Swiss National Science Foundation (NFP 47) and the European Union (TMR Quemolna MRTN-CT-2003-504880).

IC050764L